International Journal of Fracture **81:** 125–145, 1996.

Bridged versus cohesive crack in the flexural behavior of brittle-matrix composites

ALBERTO CARPINTERI[1] and ROBERTA MASSABÓ[2]
[1] *Politecnico di Torino, Department of Structural Engineering, Corso Duca degli Abruzzi 24, 10129 Torino, Italy. Phone: +39 11 5644850*
[2] *Università di Genova, Istituto di Scienza delle Costruzioni, Via Montallegro 1, 16145 Genova, Italy. Phone: +39 10 3532956; e-mail: massabo@scostr.unige.it.*

Received 26 February 1996; accepted in revised form 2 July 1996

Abstract. A nonlinear fracture mechanics model, which explains and reproduces the constitutive flexural behavior of a brittle-matrix composite, is proposed. It embraces in a unified dimensionless formulation two peculiar models, i.e., the cohesive-crack and the bridged-crack, which are used to analyze the composite failure process. Dimensionless parameters, which depend on the mechanical and geometrical properties, characterize the structure in flexure. It is shown that, based on the assumptions of the bridged-crack model, which simulates the composite as a multiphase material, the flexural response is controlled by two dimensionless parameters, whereas, based on the assumptions of the cohesive-crack model, which simulates the composite as a homogeneous material, the parameters reduce to one. The influence of the dimensionless parameters on the behavior is studied, along with the size-scale effects on the structural ductility. It is also shown how the matrix toughness affects the response. The two theoretical models are compared through the simulation of an experimental test on a fiber-reinforced beam, and it is shown that both the models can predict approximately the same overall behavior.

Key words: Fracture mechanics, fibrous composite, bridged crack, cohesive crack, size-effects.

1. Introduction

In the last decades new composite materials have been designed for utilization in different fields of engineering. Brittle ceramic matrices have been made tougher for high-technology applications through the addition of continuous or discontinuous fibers and ductile particles, and cementitious materials, used in civil engineering applications, have been reinforced with continuous or discontinuous fibers.

In spite of the profoundly different structural utilizations and the very heterogeneous mechanical and physical properties of the component materials, many similar features connect the cementitious-matrix and the ceramic-matrix composites. In particular, in both of them the fundamental role of the secondary phase is that of providing crack control and improving the fracture toughness of the brittle matrices, by means of a bridging action affecting the matrix macro- and microcracks. Debonding, sliding and frictional pulling-out of high-resistance discontinuous fibers, particles, aggregates or grains, as well as yielding or debonding of low resistance ductile particles or continuous fibers, are the local mechanisms controlling the bridging action. In the microcracked process zone ahead of the matrix macrocrack, the bridging action affects the coalescence and propagation of the microcracks, thus controlling the macrocrack extension. In the wake of the macrocrack a real stitching action prevents the crack face opening and controls the crack growth. These mechanisms increase the energy demand for the crack advancement. The matrix linear-elastic behavior is not substantially affected by low volume ratios of secondary phases, but, on the other hand, the post-cracking

response can be substantially modified, so leading to improvements in the loading capacity, ductility and durability of the structural components.

Two different nonlinear fracture mechanics models are used to analyze the composite failure process: the *bridged-crack model* and the *cohesive-crack model*, which assume, respectively, a singular and a finite stress field in the crack tip vicinity [1]. Different modeling of the composite toughening mechanisms and different crack propagation criteria are consequently assumed.

The first version of cohesive-crack model was proposed by Barenblatt [2,3], for the analysis of brittle homogeneous materials, and then by Dugdale [4], for the analysis of ductile materials. Different versions of these models were later formulated [5–15]. Many applications have regarded cementitious composites, but also other materials have been studied (e.g., polymers, metal-matrix composites).

Among the bridged-crack applications we can quote the models proposed in [16–32]. Most of these models have been related to fiber- and particle-reinforced ceramic-matrix composites, but also concrete, reinforced concrete, coarse-grained ceramics, polymers and alloys with bonded patches have been studied.

In this paper a nonlinear fracture mechanics application, which embraces in a unified dimensionless formulation the two above-mentioned peculiar models, is proposed. It analyzes the constitutive flexural response of brittle-matrix composites with uniformly distributed reinforcements. The analytical formulation derives from a model formerly proposed by Carpinteri [16] for composites with localized reinforcements. The nonlinear integral problem, describing the evolution of crack propagation in a composite section under monotonic bending, is solved through the verification of both equilibrium and kinematic compatibility. It is shown that, based on the assumptions of a nonvanishing stress intensity factor (bridged-crack) and geometric self-similarity, two dimensionless parameters control the constitutive flexural relationship. The parameters depend on the mechanical and geometrical properties. On the other hand, based on the assumption of a vanishing stress intensity factor (cohesive-crack), the number of parameters reduces to one. The size-scale effects on the structural ductility are studied, and the influence of a vanishing and a nonvanishing crack tip stress intensity factor on the constitutive relationship is examined. Finally, a bending test on a fiber reinforced mortar beam is reproduced, and it is shown that both the models can predict the same overall flexural response. A similar conclusion was reached in [33] for the tensile strength of a metal-matrix composite.

2. Theoretical assumptions: bridging and cohesive options

The proposed model explains and reproduces the constitutive monotonic flexural response of materials made with brittle matrices and continuously distributed inhomogeneities. Multiphase materials, such as ceramic or cementitious composites reinforced with continuous or discontinuous fibers or particles, as well as self-reinforced materials (concrete, coarse-grained alumina, etc.), may be considered.

The model presented here, in accordance with the ones proposed by Barenblatt [2] and Dugdale [4], replaces the bridging zone by a fictitious crack and represents the bridging actions by a closing traction distribution $\sigma_0(w)$, acting along the fictitious crack (Figure 1). The cracked cross section of a composite beam in bending is considered together with its constitutive flexural relationship evaluated by reproducing a loading process controlled by the crack advancement. This model disregards the localized action of the single reinforcements

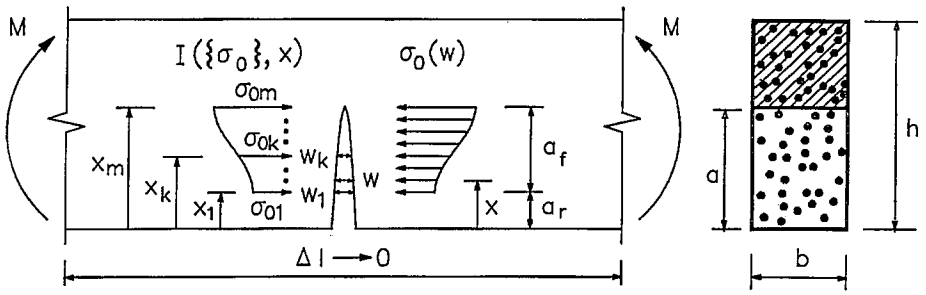

Figure 1. Schematic of the cross section.

which are homogenized in the beam volume, and therefore it cannot be used for analyses at the microscale level or for macrostructural analyses of composites with a discrete number of localized reinforcements [32, 34]. Different assumptions regarding the crack tip stress field, the consequent crack growth criterion, and the closing traction distribution are considered. These lead to the two different options of the model, which will be called *bridging option* and *cohesive option.*

In the *bridging option* the composite is theoretically simulated as a biphase material. A singular stress field is assumed at the tip of the crack and the crack starts propagating when the total crack tip stress intensity factor reaches the matrix toughness. Two distinct factors contribute to the global toughness of the composite. The first is the toughness peculiar to the matrix, which is assumed to be a material property represented by the critical stress intensity factor. The second factor is the reinforcing phase toughening mechanism, which is represented by the crack tip shielding effect that the bridging tractions develop on the crack tip stress intensification. In the bridging option the crack growth is governed by the toughness of the matrix, and the bridging tractions, which control crack opening, are governed by the properties of the reinforcing phase and by its interaction with the matrix.

In the *cohesive option*, on the other hand, the composite material is theoretically simulated as being homogeneous. A finite stress field is assumed in the crack tip vicinity, and consequently the crack starts propagating when the total crack tip stress intensity factor becomes equal to zero. This assumption is equivalent to assuming that the crack propagates when the crack tip stresses reach the composite strength, which is the value defined by the cohesive law $\sigma_0(w)$ for a zero crack opening displacement. With this option, only the global toughening mechanism of the whole composite is defined, and it is represented by the shielding effect due to the cohesive tractions. The matrix toughening mechanism, explicitly represented in the bridging option by the matrix toughness, in the cohesive option is merged with the toughening mechanism produced by the secondary phases through the cohesive law, and therefore the damage process producing the advancement of the crack is the same as that governing the opening process along the process zone.

The closing tractions present the form $\sigma_0(w) = \rho\sigma(w)$, where ρ and $\sigma(w)$ assume different meanings and values in the *bridging option* and in the *cohesive option.* In the *bridging option*, ρ is the secondary-phase volume ratio, while in the *cohesive option*, $\rho = 1$ characterizes the whole composite. The bridging or cohesive law $\sigma(w)$ is a relationship connecting the closing tractions with the crack opening displacements w along the crack faces, and it can be derived from experimental tests or micromechanical models (Figure 1). The simplest bridging

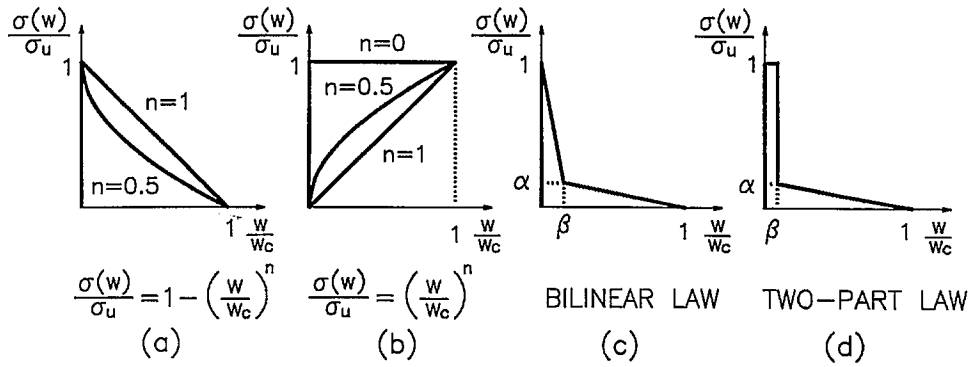

Figure 2. Analytical relationships for the description of the bridging and cohesive mechanism in brittle-matrix composites.

relationship is a rigid-perfectly plastic law which represents the bridging mechanism of ductile continuous elements, such as low-resistance fibers or wires.

More complex laws characterize the bridging mechanisms of discontinuous reinforcements, such as fibers or aggregates, or the global toughening mechanism of the homogenized composite. The relationships are in these cases characterized by a critical crack opening displacement w_c, beyond which the closing tractions vanish. The *bridging law* can be deduced from the results of pull-out tests on single fibers, for a fiber-reinforced brittle matrix material [35], whereas it is more difficult for a self-reinforced material. The *cohesive law* can be obtained by means of direct tensile tests carried out on the composite material [10], or through a theoretical simulation of these tests (see Section 6). It is usual for the cohesive law to depend on the shape and dimensions of the tested specimens.

In Figure 2 various $\sigma - w$ laws, typically used for the description of bridging and cohesive mechanisms, are shown. The law shown in Figure 2a could represent, for $n \leqslant 1$, pulling-out mechanisms against friction. The law shown in Figure 2b, could represent, for $n \leqslant 1$, bridging mechanisms due to yielding or progressive debonding of continuous fibers. The bilinear law shown in Figure 2c has been proposed by the CEB-FIP Model Code 1990 [36] for the description of the cohesive tractions in concrete. The same law, with extremely low values of the parameter β, could represent the cohesive relationship of a brittle-matrix composite with a strong secondary-phase bridging mechanism, such as a steel fiber-reinforced cementitious material [10]. The law shown in Figure 2d permits an easier numerical implementation than does the law presented in Figure 2c, and it has been used in one of the analyses proposed in the sequel.

3. Theoretical formulation

Let us examine the cracked cross section of a beam in bending shown in Figure 1. The cross-sectional depth and thickness are h and b, respectively, and the total crack depth a is given by the addition of two portions: the real or traction-free crack depth a_r, along which the crack faces have no interaction, and the fictitious crack depth a_f, upon which a closing traction distribution $\sigma_0(w)$ is active. The normalized crack depths $\xi = a/h, \xi_r = a_r/h$ and $\xi_f = a_f/h$, and the normalized coordinate $\zeta = x/h, x$ being the generic coordinate with respect to the bottom of the cross section, are defined. A two-dimensional deformation field

is assumed. The matrix is linear-elastic, both in tension and in compression, and appropriate crack propagation conditions will be assumed to describe the crack advancement.

The applied loads give rise to a singular stress field in the crack tip vicinity, which is measured by a global stress intensity factor K_I. Through the superposition principle, K_I takes on the form:

$$K_I = K_{IM} - K_{I\sigma} \tag{1}$$

where K_{IM} and $K_{I\sigma}$ are the stress intensity factors due to the bending moment M and to opening tractions $\sigma_0(w)$, respectively. In accordance with the solutions for the single-edge notched-strip [37], the stress intensity factors in eq. (1) are given by eqs. (A.1) and (A.4), shown in Appendix A.

The mobile equilibrium conditions for the crack at the onset of propagation are:

$$K_I = \begin{cases} K_{IC} & \textit{bridging option}, \quad (\textit{nonvanishing SIF}) \\ 0 & \textit{cohesive option}, \quad (\textit{vanishing SIF}). \end{cases} \tag{2}$$

Substituting eqs. (A.1) and (A.4) into eq. (2) yields:

$$\frac{M_F}{h^{1.5}b} Y_M(\xi) - h^{0.5} \int_{\xi_r}^{\xi} \sigma_0(w(\zeta)) Y_P(\xi, \zeta)\, \mathrm{d}\zeta = \begin{cases} K_{IC} \\ 0 \end{cases} \tag{3}$$

where $Y_M(\xi)$ and $Y_P(\xi, \zeta)$ are the polynomial functions shown in Appendix A. Equation (3) defines the crack propagation moment M_F, for each fixed normalized crack depth. In accordance with the dimensional analysis shown in Section 4, the dimensionless form of M_F is:

$$\frac{M_F}{K_{IC} h^{1.5} b} = \frac{1}{Y_M(\xi)} \left\{ B \int_{\xi_r}^{\xi} \frac{\sigma(w(\zeta))}{\sigma_u} Y_P(\xi, \zeta)\, \mathrm{d}\zeta + k \right\}, \tag{4}$$

Bridging option: $k = 1$

$$B = N_P = \frac{\rho \sigma_u h^{0.5}}{K_{IC}} \tag{5}$$

Cohesive option: $k = 0$

$$B = \frac{1}{s} = \frac{\sigma_u h^{0.5}}{K_{IC}}. \tag{6}$$

The constant k in the previous equations is an indication of the crack tip stress field. The parameter K_{IC} represents the matrix toughness if the crack tip stress field is singular (*bridging option*, $k = 1$). On the other hand, K_{IC} cancels on the two sides of eq. (4) if the crack tip stress field is finite (*cohesive option*, $k = 0$). In this case it can represent either the toughness of the matrix or the homogenized toughness of the composite (see Section 4.2). The constant B is an indication of the brittleness of the cross section and thus depends on the mechanical and geometrical properties of the latter. Note that in the bridging option, B is equal to the brittleness number N_P previously defined by Carpinteri [16]. N_P is the sole parameter

controlling the flexural response of composite materials reinforced with a continuous or discontinuous distribution of ductile reinforcements [34]. In the cohesive option, B is equal to the reciprocal of the brittleness number s, previously defined by Carpinteri [38] to characterize the rupture of brittle homogeneous materials. The maximum value of the bridging or cohesive stresses, $\sigma(w)$, also appears in the equations as σ_u.

The localized rotation ϕ of the cracked cross section can be evaluated using Castigliano's Theorem:

$$\phi = \frac{\partial U_F}{\partial M} \tag{7}$$

where U_F is the strain energy of the body due to the introduction of the crack, while the loads are kept constant. U_F is given as a function of the applied loads. The relationship between U_F, the generalized crack propagation force $\mathcal{G}$, the global stress intensity factor K_I, and the composite Young's modulus E is:

$$U_F = \int_0^\xi \mathcal{G} bh \, \mathrm{d}\xi = \int_0^\xi \frac{K_\mathrm{I}^2}{E} bh \, \mathrm{d}\xi. \tag{8}$$

The Poisson ratio has been assumed as negligible. Note that, for low reinforcement volume ratios, E can represent either the matrix or the composite linear-elastic behavior. Substituting eq. (8) into eq. (7) yields

$$\phi = \frac{\partial}{\partial M} \int_0^\xi \frac{K_{\mathrm{I}M}^2 + K_{\mathrm{I}\sigma}^2 - 2K_{\mathrm{I}M}K_{\mathrm{I}\sigma}}{E} bh \, \mathrm{d}\xi. \tag{9}$$

If the crack is now assumed to be at the onset of propagation, eqs. (A.1), (A.4) and (9) give the constitutive relationship, which links the localized rotation to the dimensionless crack-propagation moment:

$$\begin{aligned} \phi = \frac{2K_{\mathrm{I}C}}{Eh^{0.5}} \Bigg\{ & \frac{M_F}{K_{\mathrm{I}C}h^{1.5}b} \int_0^\xi Y_M^2(y) \, \mathrm{d}y \\ & - B \int_{\xi_r}^\xi \left(\int_{\xi_r}^y \frac{\sigma(w(\zeta))}{\sigma_u} Y_P(y,\zeta) \, \mathrm{d}\zeta \right) Y_M(y) \, \mathrm{d}y \Bigg\}. \end{aligned} \tag{10}$$

Equations (4) and (10) can be directly solved, and the constitutive flexural relationship M_F – vs. – ϕ evaluated, if the actual closing traction distribution $\sigma_0(w)$ and the normalized length of the traction-free crack ξ_r, at the lower limit of the integrals, are known. This happens if the bridging law $\sigma_0(w)$ is a rigid-perfectly plastic relationship, $\sigma_0 = \rho\sigma_u$ (see Section 4).

For a generic relationship $\sigma_0(w)$, the closing tractions are indeterminate reactions, depending on the unknown crack opening displacement function $w(x)$. The crack profile can be defined as a function of the cross section mechanical and geometrical properties and of the applied loads by means of Castigliano's Theorem:

$$w(\zeta_k) = \lim_{F \to 0} \frac{\partial}{\partial F(\zeta_k)} \left\{ \int_0^\xi \frac{K_\mathrm{I}^{f^2}}{E} bh \, \mathrm{d}\xi \right\} \tag{11}$$

where $w(\zeta_k)$ is the crack opening displacement at the generic coordinate ζ_k, F are two fictitious opening forces applied at ζ_k, and K_I^f is the global stress intensity factor, $K_I^f = K_{IM} - K_{I\sigma} + K_{IF}$, K_{IF} being the stress intensity factor due to the opening forces F, eq. (A.3). Substituting the expressions of the stress intensity factors, the normalized crack opening displacement takes on the form:

$$\tilde{w}(\zeta_k) = \frac{w(\zeta_k)}{h} = \frac{2K_{IC}}{Eh^{0.5}} \left\{ \frac{M_F}{K_{IC}h^{1.5}b} \int_{\zeta_k}^{\xi} Y_M(y) Y_P(y, \zeta_k)\, \mathrm{d}y \right. \\ \left. -B \int_{\max[\zeta_k, \xi_r]}^{\xi} \left(\int_{\xi_r}^{y} \frac{\sigma(w(\zeta))}{\sigma_u} Y_P(y, \zeta)\, \mathrm{d}\zeta \right) Y_P(y, \zeta_k)\, \mathrm{d}y \right\}. \tag{12}$$

Eqs. (4) and (12) define a nonlinear statically indeterminate problem. The indeterminate reactions $\sigma_0(w)$ are calculated using the iterative numerical procedure shown in Appendix B, which is based on the verification of equilibrium and kinematic compatibility.

4. Dimensionless parameters

In accordance with Buckingham's Theorem π of Dimensional Analysis [39], the theoretical results can be synthesized by means of functional relationships between all the physical variables involved in the flexural response of the composite material. These relationships bring out the dimensionless parameters controlling the structural response, highlight the differences between the bridging and the cohesive options of the model and define their ranges of application.

4.1. Bridging option

The *bridging option* considers both the toughening mechanism proper of the brittle matrix, controlled by the single parameter $K_{IC}[F][L]^{-1.5}$, and the toughening mechanism due to the secondary-phase bridging action. If we assume, for sake of simplicity, the bridging tractions as a power law of the crack opening displacements (Figure 2), the ultimate stress $\rho\sigma_u[F][L]^{-2}$, the critical crack opening displacement $w_c[L]$ and the exponent n of the function are the variables controlling the bridging mechanism. The crack propagation phenomenon within the beam depth, as well as the constitutive flexural response, depend on the two toughening mechanisms and on how they interact.

Equation (10), relating the cross-sectional bending moment to the localized rotation, can be put into the following general form:

$$f\left(\frac{M_F}{K_{IC}h^{1.5}b}, \phi, \frac{\rho\sigma_u h^{0.5}}{K_{IC}}, \frac{Eh^{0.5}}{K_{IC}}, \frac{w_c}{h}, n, \frac{b}{h}, \frac{a_0}{h} \right) = f(\tilde{M}, \phi, N_P, \tilde{E}, \tilde{w}_c, n; r_i) = 0 \tag{13}$$

whose terms are the variables involved, namely the dimensionless crack-propagation moment $\tilde{M}$, the localized rotation ϕ, the dimensionless ultimate stress or brittleness number N_P, the dimensionless Young's modulus $\tilde{E}$, the normalized critical crack opening displacement $\tilde{w}_c$, the exponent n of the power law and the geometrical ratios r_i, describing the shape of the cross section. The matrix toughness K_{IC} and the beam depth h have been assumed as the fundamental set of dimensionally independent variables.

The dimensionless parameters $\tilde{E}$ and $\tilde{w}_c$ are involved in the problem since the product controls the length of the traction-free crack, and therefore the lower limit of the integrals in eqs. (4) and (10), according to the kinematic condition (B.4). Consequently, if we fix the beam geometrical ratios and the exponent n of the bridging law, the structural behavior proves to be controlled by two dimensionless parameters, namely N_P and $\tilde{E}\tilde{w}_c$:

$$f(\tilde{M}, \phi, N_P, \tilde{E}\tilde{w}_c) = 0. \tag{14}$$

The theoretical model has been applied to analyze the constitutive flexural response of a composite material, whose bridging mechanism is represented by the power law $\sigma_0/\rho\sigma_u = 1 - (w/w_c)^{0.5}$. This relation might describe the bridging action of short steel fibers pulling-out from a cementitious matrix. Beams with an initial matrix crack depth $a_0 = 0.15h$, crossed by unbroken fibers, have been considered, and the constitutive relationships calculated by following the evolution of the crack up to $a = 0.95h$. The dimensionless moment-vs.-localized rotation diagrams, shown in Figs. 3a, b and c, relate to three different values of the parameter N_P, namely 0.5, 1.0 and 2.5. In each diagram a series of curves, for the parameter $\tilde{E}\tilde{w}_c$ varying from 1.0E01 to 5.0E03, is depicted.

The curve represented by dotted lines and the curve L, shown in the diagrams of Figure 3, depict two limit solutions. The former describes the constitutive behavior of the brittle matrix, and is given by the LEFM solution [37]. The latter describes the response of a composite material characterized by a very high value of the dimensionless parameter $\tilde{E}\tilde{w}_c$. It has been obtained based on the assumption of a rigid-plastic bridging law, $\sigma_0 = \rho\sigma_u$, which could represent the bridging action of long and ductile fibers. In this case, the reinforcing elements cross the crack up to total disconnection. The nonlinear problem is simply solved by checking the equilibrium condition (4), and the dimensionless parameter N_P proves to be the single governing parameter.

The curve L of Fig. 3a shows a hyper-strength phenomenon, which is an indication of a peak loading capacity that is greater than the ultimate loading capacity at complete disconnection. When the brittleness number increases, this effect turns into a snap-through instability, or a jump at constant load in a load-controlled process, as displayed by the curve L of Figure 3b. Subsequently, as the brittleness number further increases (curve L of Figure 3c), the local discontinuity disappears. This results will be explained in Section 5. The local discontinuities depend on the length of the initial matrix crack, and the snap-through instabilities would disappear if this were increased up to a limit value depending on N_P. Likewise, an initial notch, without any restraining between the crack faces, would smooth the local discontinuities.

For each fixed value N_P, the various curves in the diagrams of Figure 3 show different behaviors which represent a ductile to brittle transition when the parameter $\tilde{E}\tilde{w}_c$ decreases. For $N_P = 2.5$ strain-hardening responses are predicted for high values of $\tilde{E}\tilde{w}_c$, and strain-softening responses for low values of $\tilde{E}\tilde{w}_c$. The lower brittleness number, $N_P = 0.5$, gives rise to strain-softening responses for all the $\tilde{E}\tilde{w}_c$ examined. On the other hand, whereas the beams with high $\tilde{E}\tilde{w}_c$ are characterized by a resistance moment at complete disconnection which is greater than zero, the beams with low $\tilde{E}\tilde{w}_c$ present a zero ultimate capacity.

The influence of the fiber volume ratio ρ on the structural behavior can be investigated by varying the parameter N_P, which increases for increasing ρ, the parameter $\tilde{E}\tilde{w}_c$ being kept unchanged. If ρ is increased, the beam loading capacity heightens, the shape of the constitutive flexural relationship changes, and different transitions in the behavior are predicted based on different values of $\tilde{E}\tilde{w}_c$. If $\tilde{E}\tilde{w}_c$ presents a high value, the curves in Figure 3 represent a

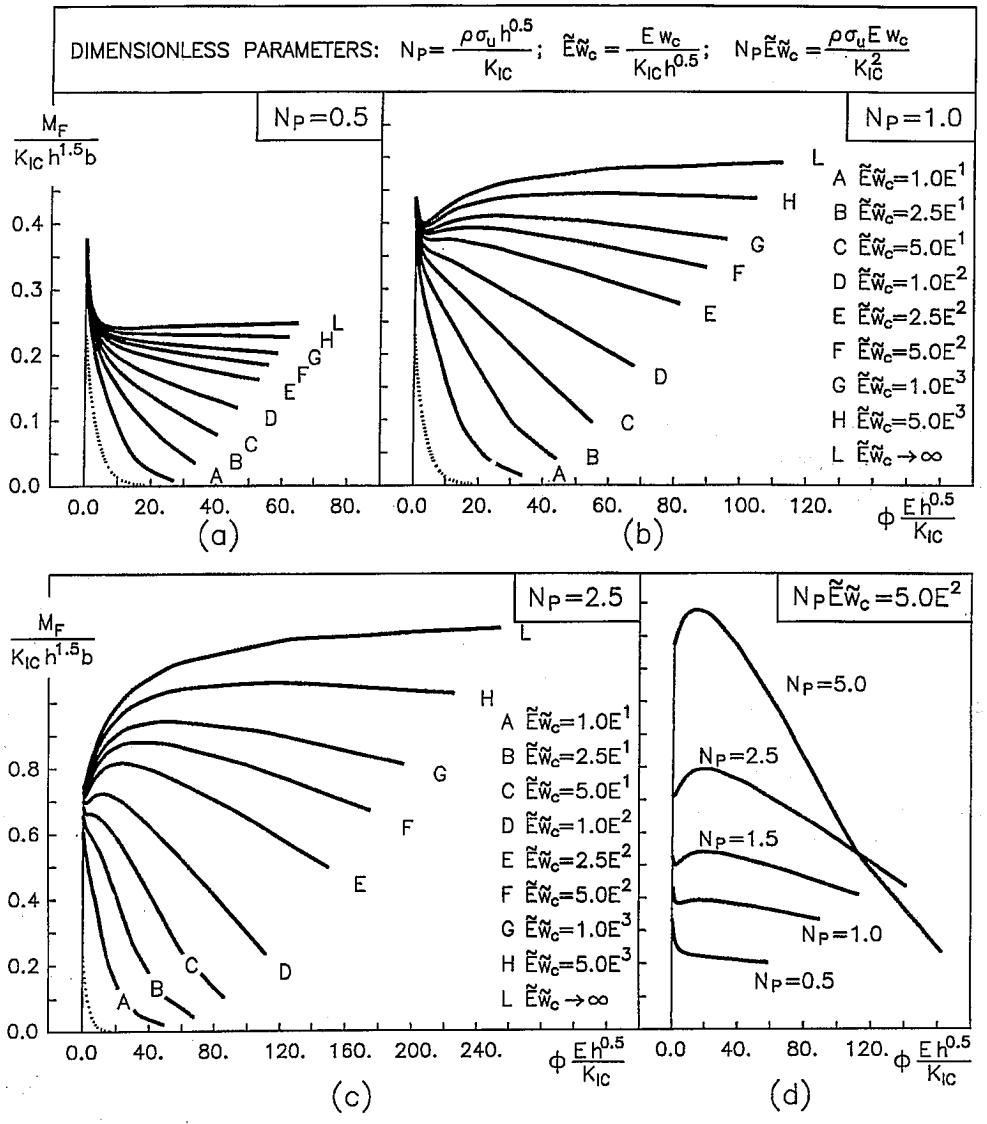

Figure 3. (a)–(c) Dimensionless crack-propagation moment versus localized rotation diagrams for a composite cross section with $N_P = 0.5, 1.0$ and 2.5, as the dimensionless parameter $\tilde{E}\tilde{w}_c$ varies (*bridging option*). (d) Dimensionless crack-propagation moment versus localized rotation curves for $N_P\tilde{E}\tilde{w}_c = 5.0E02$ and $N_P = 0.5, 1.0, 1.5, 2.5$, and 5.0.

considerable ductility of the structure (see curves L in the three diagrams). On the other hand, for low values of $\tilde{E}\tilde{w}_c$, the brittleness of the structure is high (see curves C in the three diagrams).

The dimensionless parameter $\tilde{E}\tilde{w}_c$ can be varied by varying w_c (e.g., by varying the length of short fibers). Behaviors similar to those theoretically predicted for $\tilde{E}\tilde{w}_c \to \infty$ have been experimentally detected by Jenq and Shah [21]. They tested fiber-reinforced mortar beams in flexure and observed a transition from strain-softening responses, for a very low fiber volume ratio, $\rho = 0.005$, to strain-hardening responses, for a high fiber volume ratio, $\rho = 0.015$. The

steel fibers used in the tests were 25 mm long. On the other hand, behaviors such as the ones theoretically predicted for $\tilde{E}\tilde{w}_c = 5.0\text{E}01$ have been experimentally observed in [40]. They tested a high-performance concrete reinforced with very short steel fibers, 6 mm long. Strain-softening responses were observed for all the fiber volume ratios used ($\rho = 0.03 - 0.12$), along with an embrittlement for increasing ρ.

The influence of the structural size on the constitutive relationship can be investigated by keeping the mechanical properties unchanged and varying the beam depth h. In order to do this, a constant value is assumed for the product of the two dimensionless parameters, $N_P\tilde{E}\tilde{w}_c = \rho\sigma_u E w_c/K_{IC}^2$, which does not depend on the beam depth. Different beam sizes are then considered by varying the parameter N_P.

The three curves L in Figure 3a, b, and c, obtained for a composite with long and ductile fibers ($\tilde{E}\tilde{w}_c \to \infty$), show a transition from a strain-softening response to a strain-hardening response, when N_P, and therefore the beam depth, is increased. A brittle to ductile scaling transition is predicted.

On the other hand, different values of the parameter $\tilde{E}\tilde{w}_c$ lead to different scaling transitions. The diagram shown in Figure 3d has been obtained for $N_P\tilde{E}\tilde{w}_c = 5.0\text{E}02$. The five curves in the diagram correspond to beams of different depth. A double transition, brittle to ductile to brittle, is predicted in the flexural behavior as the beam depth is increased. The beam with $N_P = 0.5$ shows a strain-softening response, the beam with $N_P = 1.0$ shows an almost perfectly plastic response, and the beam with $N_P = 5.0$ shows again a strain-softening response. Let us consider a fiber-reinforced concrete characterized by $K_{IC} = 60\,\text{Nmm}^{-1.5}, E = 50000\,\text{Nmm}^{-2}, \rho = 0.03, \sigma_u = 170\,\text{Nmm}^{-2}$, and $w_c = 10\,\text{mm}$. The curves in Figure 3d for $N_P = 0.5, 1.0, 1.5$ and 2.5 describe the flexural behavior of four beams of depths $h = 40, 140, 310$, and 850 mm, respectively. This result indicates that the behavior of a real-sized structure can be substantially different from the behavior of specimens tested in the laboratory. The experimental results obtained on small specimens cannot be extrapolated to describe larger structures.

4.2. COHESIVE OPTION

According to the *cohesive option* of the proposed theoretical model, the crack advancement in the cross section is controlled by the combined matrix-secondary phase toughening mechanism. This mechanism is represented by the shielding effect that the cohesive tractions develop on the crack tip stress intensification. Let us assume the cohesive traction $\sigma(w)$ as a function of the ultimate strength of the composite, σ_u, the critical crack opening displacement w_c, and the exponent n, according to the power laws shown in Figure 2. If geometrical similarity is assumed and the exponent n of the power law is kept constant, the functional relationship connecting the cross-sectional resistance moment with the localized rotation can be given the following form:

$$f\left(\frac{M_F}{K_{IC}h^{1.5}b}, \phi, \frac{\sigma_u h^{0.5}}{K_{IC}}, \frac{Eh^{0.5}}{K_{IC}}\frac{w_c}{h}\right) = f(\tilde{M}, \phi, s, \tilde{E}\tilde{w}_c) = 0 \tag{15}$$

in which $s = K_{IC}/(\sigma_u h^{0.5})$ is the brittleness number of eq. (6).

As previously pointed out, K_{IC} in the eqs. (4), (6) and (15), can represent either the matrix fracture toughness or the homogenized toughness of the composite. The second assumption simplifies eq. (15). The composite fracture toughness is linked, through Irwin's relationship,

to the composite fracture energy, which is defined by the area beneath the cohesive curve $\sigma(w)$. If the cohesive law $\sigma/\sigma_u = 1 - (w/w_c)^n$ is assumed, the following relationship holds:

$$\frac{K_{IC}^2}{E} = \int_0^{w_c} \sigma(w)\,\mathrm{d}w = \frac{n}{n+1}\sigma_u w_c. \tag{16}$$

By means of eq. (16), the dimensionless parameter $\tilde{E}\tilde{w}_c$ of eq. (15) can be expressed as a function of the brittleness number s. For the assumed power law the relation is:

$$\tilde{w}_c = \frac{n+1}{n}\frac{\mathcal{G}_{IC}}{\sigma_u h} = \frac{n+1}{n}\frac{s}{\tilde{E}}, \quad \text{where} \quad \mathcal{G}_{IC} = \frac{K_{IC}^2}{E}. \tag{17}$$

The dimensionless functional relationship (15) becomes:

$$f(\tilde{M}, \phi, s) = 0 \tag{18}$$

and s is the single governing parameter. Analogous arguments can be produced for any shape of the cohesive law. In the case of the power law shown in Figure 2b, for instance, the relation connecting the two parameters is $\tilde{E}\tilde{w}_c = (n+1)s$. It is worth noticing that $s = (s_E/\varepsilon_u)^{0.5}$, and also $s = (l_{ch}/2h)^{0.5}$, where s_E is Carpinteri's energy brittleness number [13], and l_{ch} is Hillerborg's characteristic length [8], ε_u being the ultimate elastic tensile strain of the composite.

In order to verify the theoretical results, a composite cross section in bending has been analyzed by means of the proposed *cohesive option*. Unlike the bridged-crack model, the cohesive-crack model has often been applied for the representation of the flexural behavior of composite beams. The flexural response of a beam in three-point bending, with a linear softening cohesive law, has been previously studied by Carpinteri [13, 41], and a ductile-brittle transition has been predicted in the behavior as the beam depth increases. Such modeling of the cohesive law could be used also for the description of a self-reinforced material, e.g., concrete.

In this application, the cohesive law shown in Figure 2d has been assumed with $\alpha = 0.1$ and $\beta = 0.001$. This law might represent the cohesive mechanism of a steel-fiber cementitious material. The first part of the relationship describes the matrix toughness and the second part the toughening mechanism of the secondary phases.

The moment versus localized rotation dimensionless diagrams in Figure 4 have been obtained by analyzing a cross section with an initial crack depth of $a_0 = 0.05h$, for six different brittleness numbers, i.e., $s = 5.0, 1.0, 0.7, 0.5, 0.3$ and 0.2. For $s = 5.0$ the cross section is characterized by a strain-softening response, for $s = 0.7$ an almost strain-hardening response is predicted and for brittleness numbers lower than $s = 0.5$ the behavior becomes again globally strain-softening. The cohesive option, therefore, reproduces the same size-scale effect previously observed in Figure 3d for the bridging option results, according to which a double transition is predicted when the beam depth is increased.

Note that the double transition, the local discontinuities and the hyper-strength phenomena shown by the curves in Figure 4 are due to the particular choice of the cohesive law, and these phenomena would not be predicted if the cohesive relationship were characterized by a generic power law.

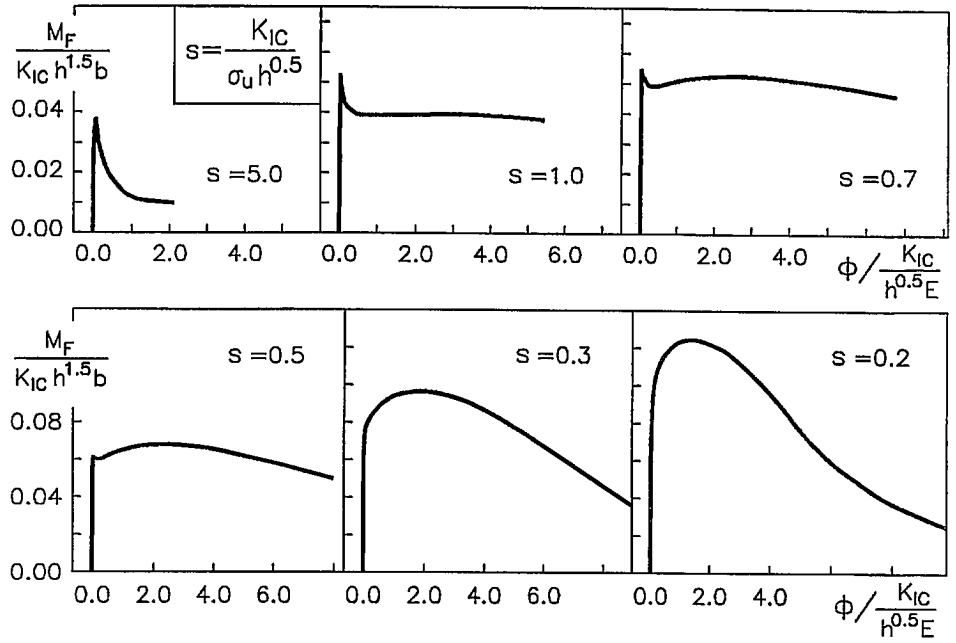

Figure 4. Dimensionless crack-propagation moment versus localized rotation diagrams for a composite cross section as the brittleness number s varies (*cohesive option*).

5. Influence of matrix toughness on structural response

Under particular conditions, the influence of matrix toughness on structural response may be neglected and therefore, provided the cohesive and the bridging laws coincide, the model options both predict the same global results. Let us consider, for sake of simplicity, a composite material whose secondary-phase bridging mechanism can be simulated through a rigid-plastic bridging relationship, $\sigma_0(w) = \rho\sigma_u$. The mechanical behavior of a cross section in bending, with an initial matrix crack of depth $a_0 = 0.1h$, has been evaluated by means of the bridging option of the proposed theoretical model (nonvanishing stress intensity factor). Three different brittleness numbers have been assumed, namely $N_P = 0.5, 1.1$ and 2.5. Then, the cohesive option has been applied (vanishing stress intensity factor), with a cohesive law coincident with the previously assumed bridging law. In this way, the flexural response of the composite material can be studied disregarding the effects of the matrix toughness.

In order to make a direct comparison of the two model options, a new set of dimensionally independent variables, $\rho\sigma_u[F][L]^{-2}$ and $h[L]$, has been chosen, and eqs. (4) and (10) have been worked out arriving at the dimensionless relationship connecting $M/(\rho\sigma_u h^2 b)$ with $\phi/(\rho\sigma_u E^{-1})$, in which the matrix toughness is absent.

In the diagram of Figure 5, the constitutive curves obtained by the application of the bridging and cohesive options are represented by the thin and thick curves, respectively. The thick curve is the same in all diagrams and define a strain-hardening response, whereas the thin curves show the transition previously observed in the curves L of Figure 3.

The ultimate moments, for the totally disconnected sections, are the same for both the model options, as they are not affected by the matrix toughness which, on the other hand, strongly controls the remaining part of the curves. For high values of N_P, the cohesive option

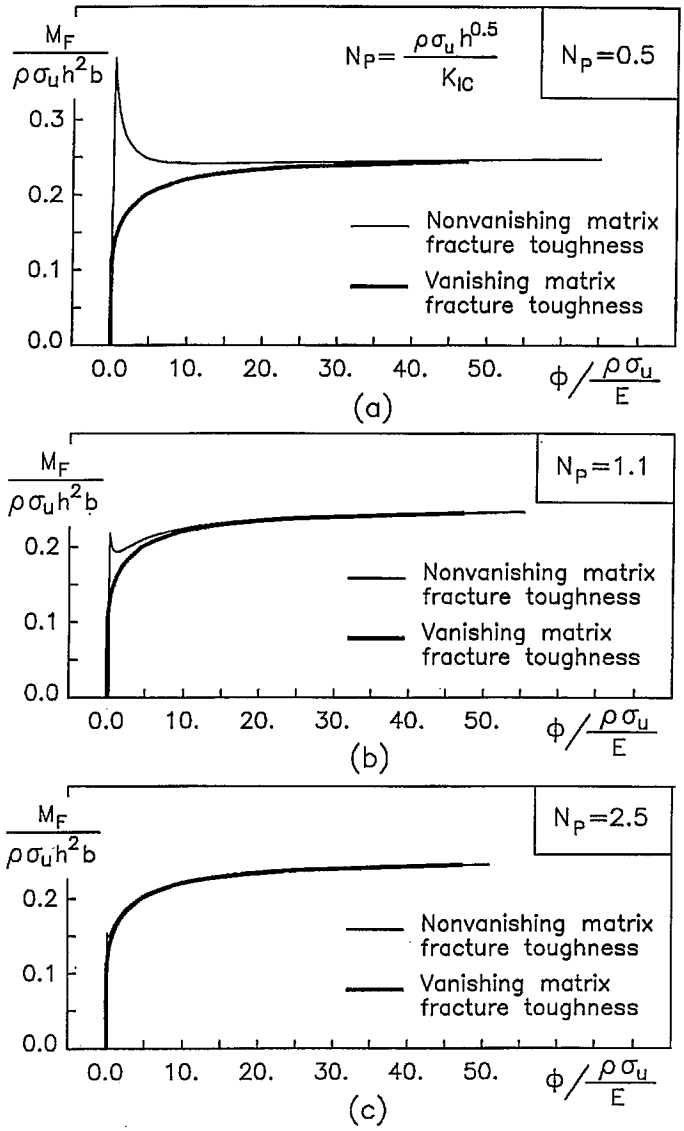

Figure 5. Dimensionless crack-propagation moment versus localized rotation diagrams for a composite cross section with $N_P = 0.5$, 1.1 and 2.5, and a rigid-plastic bridging relationship. Comparison between the constitutive curves predicted by considering or not the matrix fracture toughness.

and the bridging option predict almost the same global response, which is therefore merely controlled by the toughening action of the reinforcing elements. This situation can be obtained for large beams or when the material properties are characterized by a low ratio $K_{IC}/(\rho\sigma_u)$. On the other hand, for the lower brittleness numbers the matrix toughness strongly affects the structural performance during the entire loading phase. This situation characterizes shallow beams or composites with a high ratio $K_{IC}/(\rho\sigma_u)$. A different choice of the bridging law would modify the results shown in Figure 5, but the general considerations continue to hold good.

In conclusion, if disregarding the matrix toughness does not affect the quality of the results in the theoretical simulation of the mechanical behavior of a composite element whose brittleness number N_P is high, the same assumption, in a composite with a low N_P, will induce an underestimation of the cross section loading capacity and an erroneous prediction of the shape of the flexural constitutive curve. To overcome this problem, the toughening mechanism peculiar to the matrix has to be merged with the toughening mechanism due to the secondary phases, through the definition of a proper cohesive law (see next section).

6. Bridged versus cohesive crack

Willis [6] proved the equivalence between Barenblatt's cohesive-crack model for brittle materials and Griffith's criterion [42]. This result derives from Barenblatt's assumption of a crack-edge region, acted upon by the forces of cohesion, which is negligibly small compared to the entire area of the crack surface, and proves the equivalence of the cohesive-crack model with the bridged-crack model in the limit case of a brittle material, i.e., when secondary phases are absent. In this section it will be shown that the same results can be obtained for a brittle-matrix composite.

An experimental three point bending test, carried out by Jenq and Shah [21] on a fiber-reinforced mortar beam, has been considered. The beam had a depth × thickness × span of $76 \times 19 \times 280$ mm and a notch of depth $a_0 \simeq 25$ mm. The unreinforced matrix toughness has been evaluated by Jenq and Shah as equal to $K_{IC} = 27.5\,\mathrm{N\,mm^{-1.5}}$. Brass-coated smooth steel fibers, 25 mm long and with a 0.4 mm diameter, were used in a volume ratio $\rho = 0.005$. A pull-out test on a single, aligned fiber, had shown a typical response controlled by the frictional pulling out of the fiber from the matrix with a maximum pull-out strength σ_u of $169\,\mathrm{N\,mm^{-2}}$.

The *bridging option* of the proposed theoretical model has been applied to simulate the experimental test. The option entails the definition of the shape of the fiber bridging law $\sigma_0(w)$, and the parameters N_P and $\tilde{E}\tilde{w}_c$. The bridging law has been deduced by simply extrapolating to the whole of the fibers the pull-out relationship experimentally displayed by a single fiber, $\sigma_0(w) = \rho\sigma(w)$. The power law $\sigma/\sigma_u = (1 - w/w_c)^{0.5}$ [21], with the critical crack opening displacement equal to half the fiber length $w_c = 12.5$ mm, has been assumed. The assumption disregards the fiber volumetric distribution and orientation with respect to the crack faces. The elastic modulus of the composite has been assumed equal to $22000\,\mathrm{N\,mm^{-2}}$, from the analysis of the linear-elastic branch of the experimental load-deflection curve, and the dimensionless parameters turn out to be $N_P = 0.27$ and $\tilde{E}\tilde{w}_c = 1148$.

In order to evaluate the beam load-displacement curve, the flexural constitutive relationship, defined by eqs. (4) and (10), has been used to characterize a nonlinear hinge placed in the middle free span of a three-point bending linear-elastic beam.

In Figure 6a a comparison between the experimental load versus displacement curve and the theoretical one is shown. The theoretical model reproduces the actual response consistently, both in the strain softening branch, during unstable crack propagation, and in the ultimate loading capacity.

The application of the *cohesive option* entails the definition of the shape of the cohesive law and the dimensionless parameter s. The cohesive law could be experimentally defined through a direct tension test on the composite material. It can also be defined by applying the bridging option of the proposed model in order to provide a theoretical simulation of that test, provided the fiber-bridging law and the matrix toughness are known. By means of this simulation, on a double-edge notched specimen, the relationship linking the applied

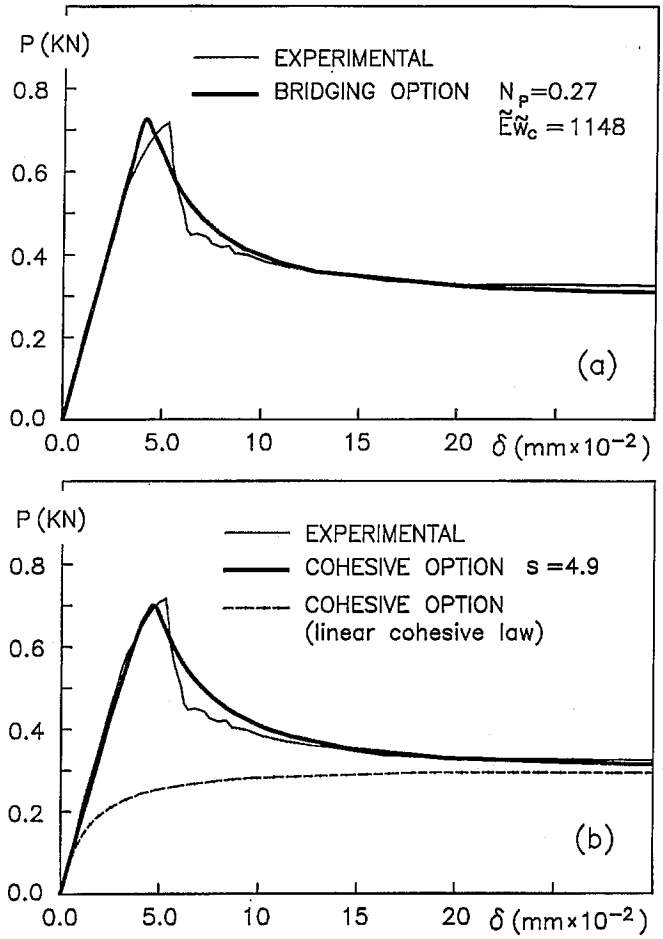

Figure 6. (a) Comparison between the load-deflection experimental curve of a fiber-reinforced mortar beam, after Jenq and Shah [21], and the theoretical results (bridging option). (b) Comparison between the load-deflection experimental curve and the theoretical results (cohesive option).

stress to the relative displacements around the cracked cross section of the specimen has been evaluated and assumed as the cohesive law of the composite material. As a rough approximation of the resulting stress-displacement curve, characterized by a rapid drop and an extended tail, the bilinear function shown in the diagram of Figure 3c has been used assuming $\sigma_u = 8.0\,\mathrm{N\,mm^{-2}}, w_c = 12.5\,\mathrm{mm}, \alpha\sigma_u = 0.84\,\mathrm{N\,mm^{-2}}$ and $\beta w_c = 1.0 \times 10^{-2}\,\mathrm{mm}$. The brittleness number s, through eq. (6), is $s = 4.9$. Note that K_{IC} represents in this case the homogenized toughness, given by the area under the cohesive curve.

In Figure 6b the theoretical load-displacement curve is compared with the experimental results. A good agreement is found and it is shown that the cohesive option can better reproduce the first microcracking phase preceding the maximum load, than can the bridging option. Nevertheless, it is worth noting that the computational problems connected with the cohesive-crack model, if a cohesive law of the kind assumed in this application is used, are far more complicated than the ones connected with the bridged-crack model.

The importance of a proper definition of the bridging and cohesive laws, sharp variations and discontinuities included, is made evident by the dashed curve in the diagram of Figure 6b. The curve has been obtained by assuming a cohesive law which disregards the peak of the previously assumed bilinear law of Figure 3c. This assumption implies disregarding the effects of the matrix toughness on the structural behavior. The completely erroneous prediction confirms the results of the previous section. For low brittleness numbers, in this example $N_P = 0.27$, the loading capacity of the beam is strongly affected by the matrix toughness. This behavior depends on both the material properties and the structure geometry. The influence of the matrix toughness on the peak-load would mitigate in larger beams (higher N_P).

The above application has shown that the parameters characterizing the cohesive option of the theoretical model can be deduced from an application of the bridging option, once the geometrical dimensions of the member are fixed and the matrix toughness and the fiber-bridging mechanism are known. On the other hand, the parameter characterizing the bridging option cannot be deduced from the cohesive option, as many different bridging mechanisms and different combinations of the matrix toughness and the bridging tractions may exist which lead to the same cohesive law.

7. Conclusions

A nonlinear fracture mechanics application has been proposed which fits in a unified dimensionless formulation the two peculiar models used to analyze the failure processes in brittle-matrix composites (i.e., bridging-crack and cohesive crack model). The bridged-crack model assumes a singular stress field in the crack tip vicinity, represents the brittle-matrix toughness by a critical stress intensity factor, and simulates the secondary-phase restraining of crack propagation through a closing traction distribution directly applied along the faces of a fictitious crack. The cohesive-crack model, on the other hand, assumes a finite stress field in the crack tip vicinity and the closing tractions represent in this case the combined matrix-secondary phase resistance against crack propagation. An appropriate bridging law or cohesive law, linking the closing tractions to the crack opening displacements, is assigned as a datum of the problem.

The constitutive flexural relationship of a generic brittle-matrix composite can be evaluated and, if geometrical similarity is assumed, the structural response proves to be controlled by certain dimensionless parameters, which depend on the mechanical and geometrical properties. Based on the assumptions of the bridged crack model, the number of governing dimensionless parameters is two, whereas, based on the assumptions of the cohesive-crack model, this number reduces to one. It has also been shown that the parameters of the cohesive model (shape of the cohesive law and brittleness number s) can be deduced by a proper application of a bridged-crack model. The different models of the composite material explain these results. The bridging option, in fact, analyzes the composite as a real biphase material, whereas the cohesive option renders homogeneous the different phases.

The influence of the beam depth on the constitutive relationship has been studied, and different scaling transitions predicted according to different values of the dimensionless parameters. Finally, it has been shown, by a comparison with the results of an experimental test on a fiber-reinforced mortar beam, that, if the dimensionless parameters and the bridging and cohesive laws are properly defined, the proposed models converge approximately to the same global result.

A. Appendix

$$K_{IM} = \frac{M}{h^{1.5}b} Y_M(\xi), \tag{A.1}$$

where:

$$Y_M(\xi) = \begin{cases} 6(1.99\xi^{0.5} - 2.47\xi^{1.5} + 12.97\xi^{2.5} - 23.17\xi^{3.5} + 24.8\xi^{4.5}), \xi \leqslant 0.6 \\ \dfrac{3.99}{(1-\xi)^{1.5}}, \xi \geqslant 0.6 \end{cases} \tag{A.2}$$

$$K_{IF} = \frac{F}{h^{0.5}b} Y_P(\xi, \zeta), \tag{A.3}$$

$$K_{I\sigma} = \int_{\xi_r}^{\xi} \frac{K_{IF}}{F} \sigma_0(w(\zeta)) bh \, \mathrm{d}\zeta = \frac{1}{h^{0.5}b} \int_{\xi_r}^{\xi} \sigma_0(w(\zeta)) Y_P(\xi, \zeta) bh \, \mathrm{d}\zeta, \tag{A.4}$$

where:

$$\begin{aligned} Y_P(\xi,\zeta) &= \frac{2}{\sqrt{\pi\xi}} \frac{1}{(1-\xi)^{1.5}\sqrt{1-(\frac{\zeta}{\xi})^2}} G(\xi,\zeta), \\ G(\xi,\zeta) &= g_1(\xi) + g_2(\xi)\frac{\zeta}{\xi} + g_3(\xi)\frac{\zeta^2}{\xi} + g_4(\xi)\frac{\zeta^3}{\xi}, \\ g_1(\xi) &= 0.46 + 3.06\xi + 0.84(1-\xi)^5 + 0.66\xi^2(1-\xi)^2 \\ g_2(\xi) &= -3.52\xi^2 \\ g_3(\xi) &= 6.17 - 28.22\xi + 34.54\xi^2 - 14.39\xi^3 - (1-\xi)^{1.5} \\ &\quad -5.88(1-\xi)^5 - 2.64\xi^2(1-\xi)^2 \\ g_4(\xi) &= -6.63 + 25.16\xi - 31.04\xi^2 + 14.41\xi^3 + 2(1-\xi)^{1.5} \\ &\quad +5.04(1-\xi)^5 + 1.98\xi^2(1-\xi)^2. \end{aligned} \tag{A.5}$$

B. Appendix

A discrete number n of points are defined along the faces of the crack shown in Figure 1 through the position vector $\{\zeta\} = \{\zeta_1, \ldots, \zeta_n\}^T, \zeta_i = x_i/h$ being the generic normalized coordinate with respect to the bottom of the cross section. The crack opening displacement vector $\{w\} = \{w_1(\zeta_1), \ldots, w_n(\zeta_n)\}^T$ and its normalized form $\{\tilde{w}\} = \{\tilde{w}_1, \ldots, \tilde{w}_n\}^T$, whose generic component is $\tilde{w}_i = w_i/h$, are defined. Moreover, the corresponding closing traction vector $\{\sigma_0\} = \{\sigma_{01}(w_1), \ldots, \sigma_{0n}(w_n)\}^T$, whose components are the closing traction values in the n points, is considered.

The nonlinear analysis is formulated in a matrix form, and the bridging law $\sigma_0(w)$ is replaced by an interpolating function $I(\{\sigma_0\}, \zeta)$, which depends on the closing traction vector $\{\sigma_0\}$ and on the normalized coordinate ζ (Figure 1). This function is obtained by interpolating

over the values of $\sigma_0(w)$ in the n points along the crack, according to the vector $\{\sigma_0\}$. In view of the sharp variations that $\sigma_0(w)$ can exhibit, a suitable interpolation is achieved using cubic splines, and the function $I(\{\sigma_0\},\zeta)$ is thus represented by $n-1$ third-order polynomials $I_j(\{\sigma_0\},\zeta), j=1,\ldots,(n-1)$, attached together in the n points along the crack without any discontinuities [29]. The jth polynomial $I_j(\{\sigma_0\},\zeta)$, spanning the coordinates ζ_j and ζ_{j+1}, takes on the form:

$$I_j(\{\sigma_0\},\zeta) = c_{j0} + \sum_{l=1}^{3} c_{jl}(\zeta-\zeta_j)^l, \qquad \zeta_j \leqslant \zeta \leqslant \zeta_{j+1}. \tag{B.1}$$

The $n-1$ coefficients c_{j0} equalize the components of the vector $\{\sigma_0\}$, $c_{j0}=\sigma_{0j}$, according to the interpolation condition. The remaining $3(n-1)$ coefficients c_{jl} are evaluated by means of continuity conditions in the n points. The iterative procedure is constituted by the following steps.

1. The total crack depth a and its normalized value $\xi = a/h$ are fixed and the closing traction relationship $\sigma_0(w)$ is assigned.

2. A tentative profile is assumed, through the definition of a starting displacement vector $\{w^i\} = \{w_1^i(\zeta_1),\ldots,w_n^i(\zeta_n)\}^T$, i being the iteration index. A linear function of the coordinate ζ can for example be established, this implying plane crack faces. The normalized real crack depth $\xi_r^i = a_r^i/h$, at the tip of which the crack opening displacement reaches the critical value $w_r^i = w_c$, and the normalized fictitious crack depth $\xi_f^i = a_f^i/h$, are consequently fixed.

3. The closing traction vector $\{\sigma_0^i\} = \{\sigma_0^i(w_1^i),\ldots,\sigma_0^i(w_n^i)\}^T$ is defined by means of the assigned relationship $\sigma_0(w)$. Moreover the interpolating function $I^i(\{\sigma_0^i\},\zeta)$ is evaluated through eq. (B.1).

4. Equilibrium condition. The applied moment of crack propagation M_F^i, which corresponds, together with the assumed closing tractions, to the crack in a state of mobile equilibrium, is evaluated through the crack propagation condition (2). By taking advantage of eqs. (4) and (B.1), it is found

$$\frac{M_F^i}{K_{IC}h^{1.5}b} = \frac{1}{Y_M(\xi)}\left\{B\sum_{j=1}^{n-1}\int_{\zeta_j}^{\zeta_{j+1}}\frac{I_j^i(\{\sigma^i\},\zeta)}{\sigma_u}Y_P(\xi,\zeta)\,\mathrm{d}\zeta + k\right\}, \tag{B.2}$$

in which B and k have been previously defined in eqs. (5) and (6), and the summation is on the $n-1$ polynomials constituting the interpolating function.

5. The crack opening displacement vector $\{w^{i+1}\}$, in the equilibrium state at the onset of crack propagation, is evaluated. The generic kth component, normalized with respect to the cross section depth h, takes the form:

$$\tilde{w}_k^{i+1} = \frac{w_k^{i+1}}{h} = \frac{2K_{IC}}{Eh^{0.5}}\left\{\frac{M_F^i}{K_{IC}h^{1.5}b}\int_{\zeta_k}^{\xi} Y_M(y)Y_P(y,\zeta_k)\,\mathrm{d}y\right.$$

$$\left. -B\sum_{j=1}^{n-1}\int_{\max[\zeta_k,\zeta_j]}\left(\int_{\zeta_j}^{\min[y,\zeta_{j+1}]}\frac{I_j^i(\{\sigma^i\},\zeta)}{\sigma_u}Y_P(\bar{\zeta},\zeta)\,\mathrm{d}\zeta\right)Y_P(y,\zeta_k)\,\mathrm{d}y\right\} \tag{B.3}$$

in which $\bar{\zeta} = \min[y,\zeta_{j+1}]$.

6. Compatibility verification. The solution of the problem, represented by Equations (B.2) and (B.3), which meets the equilibrium condition, does not necessarily fulfill the kinematic requirements, as the calculated crack opening displacement vector $\{w^{i+1}\}$, eq. (B.3), can be different from the assumed one $\{w^i\}$. Two different checks are performed. The first check concerns the evaluated normalized length of the traction free crack ξ_r^{i+1}, which defines the coordinates where the crack opening displacement has reached its critical value, $\tilde{w}_r^{i+1} = \tilde{w}_c$. By taking advantage of eq. (B.3), at the tip of the traction-free crack the following condition has to be satisfied:

$$\frac{M_F^i}{K_{IC}h^{1.5}b}\int_{\xi_r}^{\xi} Y_M(y)Y_P(y,\xi_r)\,\mathrm{d}y$$

$$-B\sum_{j=1}^{n-1}\int_{\max[\xi_r,\zeta_j]}^{\xi}\int_{\zeta_j}^{\min[y,\zeta_{j+1}]}\frac{I_j^i(\{\sigma^i\},\zeta)}{\sigma_u}Y_P(\bar{\zeta},\zeta)\,\mathrm{d}\zeta Y_P(y,\xi_r)\,\mathrm{d}y = \tfrac{1}{2}\tilde{E}\tilde{w}_c. \qquad \text{(B.4)}$$

The calculated traction-free crack length ξ_r^{i+1} is then compared with the assumed value ξ_r^i. The second check is developed by comparing the norm of the difference vector $\{w^{i+1}\} - \{w^i\}$ with the norm of the assumed vector $\{w^i\}$. If the convergence is reached, the compatibility is verified and the iterative procedure stops. Otherwise, a new iteration $i+1$ is performed, starting again from point (3), with the new shape of the crack faces defined by $\{w^{i+1}\}$.

7. Structural behavior. After reaching convergence, the structural behavior can be completely characterized by means of the relationships linking the crack-propagation moment to the crack depth and to the localized rotation due to the crack. The final expression of the localized rotation due to the crack, is given by

$$\phi = \frac{2K_{IC}}{Eh^{0.5}}\left\{\frac{M_F}{K_{IC}h^{1.5}b}\int_0^{\xi} Y_M^2(y)\,\mathrm{d}y\right.$$

$$\left. - B\sum_{j=1}^{n-1}\int_{\zeta_j}^{\xi}\left(\int_{\zeta_j}^{\min[y,\zeta_{j+1}]}\frac{I_j(\{\sigma\},\zeta)}{\sigma_u}Y_P(\bar{\zeta},\zeta)\,\mathrm{d}\zeta\right)Y_M(y)\,\mathrm{d}y\right\}, \qquad \text{(B.5)}$$

in which $\bar{\zeta} = \min[y, \zeta_{j+1}]$. The constitutive flexural relationship can be defined by progressively increasing the total crack depth at point (1), so as to cover the entire beam depth.

Acknowledgements

The authors gratefully acknowledge the financial support of the National Research Council (CNR) and the Department for the University and for Scientific and Technological Research (MURST).

References

1. B.N. Cox and D.B. Marshall, Concepts for bridged cracks in fracture and fatigue, *Acta Metallurgica Materialia* 42(2), (1994), 341–363.
2. G.I. Barenblatt, The formation of equilibrium cracks during brittle fracture. General ideas and hypotheses. Axially-symmetric cracks, *Journal of Applied Mathematics and Mechanics* 23(3), (1959), 622–636.
3. G.I. Barenblatt, The mathematical theory of equilibrium cracks in brittle fracture, in H.L. Dryden and T. von Karman (eds), *Advances in Applied Mechanics*, Academic Press, New York (1962), 55–129.

4. D.S. Dugdale, Yielding of steel sheets containing slits, *Journal of Mechanics and Physics of Solids* 8(2), (1960), 100–104.
5. B.A. Bilby, A.H. Cottrell and K.H. Swinden, The spread of plastic yield from a notch, *Proceedings Royal Society of London* A272 (1963), 304–314.
6. J.R. Willis, A comparison of the fracture criteria of Griffith and Barenblatt, *Journal of Mechanics and Physics of Solids* 15 (1967), 151–162.
7. J.R. Rice, A path independent integral and the approximate analysis of strain concentration by notches and cracks, *Journal of Applied Mechanics* 35 (1968), 379–386.
8. A. Hillerborg, M. Modeer and P.E. Petersson, Analysis of crack formation and crack growth in concrete by means of fracture mechanics and finite elements, *Cement and Concrete Research* 6(6), (1976), 773–782.
9. R. Ballarini, S.P. Shah and L.M. Keer, Crack growth in cement-based composites, *Engineering Fracture Mechanics* 20(3), (1984), 433–445.
10. V.C. Li and E. Liang, Fracture processes in concrete and fiber reinforced cementitious composites, *Journal of Engineering Mechanics* 112(2), (1986), 566–586.
11. S.P. Shah, Fracture toughness of cement-based materials, *Materials and Structures* 21(122), (1988), 145–150.
12. T. Ungsuwarungsri and W.G. Knauss, Nonlinear analysis of an equilibrium craze: part I-problem formulation and solution, *Journal of Applied Mechanics* 55 (1988), 44–51.
13. A. Carpinteri, Cusp catastrophe interpretation of fracture instability, *Journal of Mechanics and Physics of Solids* 37(5), (1989), 567–582.
14. E. Smith, The size of the fully developed softening zone associated with a crack in a strain-softening material-I. A semi-infinite crack in a remotely loaded infinite solid, *International Journal Engineering Science* 27(3), (1989), 301–307.
15. B. Cotterell, P. Paramasivam and K.Y. Lam, Modeling the fracture of cementitious materials, *Materials and Structures* 25(145), (1992), 14–20.
16. A. Carpinteri, Stability of fracturing process in r.c. beams, *Journal of Structural Engineering* 110(3), (1984), 544–558.
17. Y.S. Jenq and S.P. Shah, Two parameter fracture model for concrete, *Journal of Engineering Mechanics* 111(10), (1985), 1227–41.
18. D.B. Marshall, B.N. Cox and A.G. Evans, The mechanics of matrix cracking in brittle-matrix fiber composites, *Acta Metallurgica Materialia* 33 (1985), 2013–2021.
19. B. Budiansky, J.W. Hutchinson and A.G. Evans, Matrix fracture in fiber-reinforced ceramics, *Journal of Mechanics and Physics of Solids* 34 (1986), 167–189.
20. R.M.L. Foote, Y.-W. Mai and B. Cotterell, Crack growth resistance curves in strain-softening materials, *Journal of Mechanics and Physics of Solids* 34(6), (1986), 593–607.
21. Y.S. Jenq and S.P. Shah, Crack propagation in fiber-reinforced concrete, *Journal of Structural Engineering* 112(1), (1986), 19–34.
22. L.R.F. Rose, Influence of debonding on the efficiency of crack patching, *Theoretical and Applied Fracture Mechanics* 7 (1987), 125–132.
23. P.L. Swanson, C.J. Fairbanks, B.R. Lawn, Y.W. Mai and B.J. Hockey, Crack interface grain bridging as a fracture resistance mechanism in ceramics: II, theoretical fracture mechanics model, *Journal of American Ceramic Society* 70 (1987), 289–294.
24. F. Erdogan and P.F. Joseph, Toughening of ceramics through crack bridging by ductile particles, *Journal of American Ceramic Society* 72 (1989), 262–270.
25. R. Ballarini and S. Muju, Stability analysis of bridged cracks in brittle matrix composites, *Journal of Engineering Gas Turbines Power* 115 (1993), 127–138.
26. H.A. Luo and R. Ballarini, The effects of anisotropy on the nonlinear behavior of bridged cracks in long strips, *Journal of Mechanics and Physics of Solids* 42 (1994), 141–157.
27. K. Kendall, W.J. Clegg and R.D. Gregory, Growth of tied cracks: a model for polymer crazing, *Journal Material Science Letter* 10 (1991), 671–674.
28. B.N. Cox, Extrinsic factors in the mechanics of bridged cracks, *Acta Metallurgica Materialia* 39 (1991), 1189–1201.
29. B.N. Cox and D.B. Marshall, Stable and unstable solutions for bridged cracks in various specimens, *Acta Metallurgica Materialia* 39 (1991), 579–589.
30. C. Bosco and A. Carpinteri, Softening and snap-through behavior of reinforced elements, *J. Engineering Mechanics* 118(8), (1992), 1564–1577.
31. B.N. Cox and C.S. Lo, Load ratio, notch, and scale effects for bridged cracks in fibrous composites, *Acta Metallurgica Materialia* 40 (1992), 69–80.
32. C. Bosco and A. Carpinteri, Discontinuous constitutive response of brittle matrix fibrous composites, *Journal of Mechanics and Physics of Solids* 43(2), (1995), 261–274.

33. S.J. Connel, F.W. Zok, Z.Z. Du and Z. Suo, On the tensile properties of a fiber reinforced titanium matrix composite-II. Influence of notches and holes, *Acta Metallurgica Materialia* 42(10), (1994), 3451–3461.
34. A. Carpinteri and R. Massabó, Continuous versus discontinuous bridged crack model for fiber-reinforced materials in flexure, *International Journal of Solids and Structures*, in press.
35. A. Burakiewicz, Testing of fiber bond strength in cement matrix, in Swamy (ed.). *Testing and test methods of fiber cement composites*, The Construction Press Ltd, Lancaster, U.K., (1978), 355–369.
36. Comite Euro-International du Beton: CEB-FIB Model Code 1990, *CEB Bulletin d'Information*, Vol. 213–214 (1993).
37. H. Tada, P.C. Paris and G. Irwin, *The Stress Analysis of Cracks Handbook*, Paris Productions Incorporated (and Del Research Corporation), St. Louis, Missouri (1985).
38. A. Carpinteri, Static and energetic fracture parameters for rocks and concretes, *Materials and Structures* 14(81), (1981), 151–162.
39. E. Buckingham, Model experiments and the form of empirical equations, *Transactions ASME* 37 (1915), 263–296.
40. P. Tjiptobroto and W. Hansen, Tensile strain hardening and multiple cracking in high-performance cement-based composites containing discontinuous fibers, *ACI Material Journal* 90(1), (1993), 16–25.
41. A. Carpinteri, Size-scale transition from ductile to brittle failure: structural response vs. crack growth resistance curve, *International Journal of Fracture* 51 (1991), 175–186.
42. A.A. Griffith, The phenomena of rupture and flow in solids, *Philosophical Transactions Royal Society London* A221 (1921), 163–198.